EFDA–JET–PR(12)30

P.C. de Vries, A.C.C. Sips, H.T. Kim, P.J. Lomas, F. Maviglia, R. Albanese, I. Coffey, E. Joffrin, M. Lehnen, A. Manzanares, M. O'Mulane, I. Nunes, G. van Rooij, F.G. Rimini, M.F. Stamp and JET EFDA contributors

Characterisation of Plasma Breakdown at JET with a Carbon and ITER-like Wall

Characterisation of Plasma Breakdown at JET with a Carbon and ITER-like Wall

P.C. de Vries[1], A.C.C. Sips[2,3], H.T. Kim[4,5], P.J. Lomas[4], F. Maviglia[6], R. Albanese[6], I. Coffey[7], E. Joffrin[8], M. Lehnen[9], A. Manzanares[10], M. O'Mulane[4], I. Nunes[2,11], G. van Rooij[1], F.G. Rimini[4], M.F. Stamp[4] and JET EFDA contributors*

JET-EFDA, Culham Science Centre, OX14 3DB, Abingdon, UK

[1]*FOM institute DIFFER, Association EURATOM-FOM, P.O. Box 1207, 3430BE Nieuwegein, Netherlands*
[2]*European Commission, Brussels, Belgium*
[3]*EFDA-CSU, Culham Science Centre, OX14 3DB Abingdon, UK*
[4]*EURATOM-CCFE Fusion Association, Culham Science Centre, OX14 3DB, Abingdon, OXON, UK*
[5]*Department of Physics, Imperial College London, SW7 2AZ, London, UK.*
[6]*Associazione EURATOM-ENEA-CREATE, Univ. di Napoli Federico II, Napoli, Italy.*
[7]*Queen's University Belfast, BT71NN, UK*
[8]*CEA-IRFM, Association Euratom-CEA , Cadarache, F-13108, France.*
[9]*Institut für Energie- und Klimatforschung-IEK-4, Forschungszentrum Jülich GmbH, EURATOM Association, 52425 Jülich, Germany.*
[10]*Laboratorio Nacional de Fusión, EURATOM-CIEMAT Association, Madrid, Spain*
[11]*Associação EURATOM-IST, Instituto de Plasmas e Fusão Nuclear, Lisboa, Portugal.*
(24th IAEA Fusion Energy Conference, San Diego, USA (2012)).

Preprint of Paper to be submitted for publication in
Nuclear Fusion

ABSTRACT

The recent installation of a full metal, ITER-like, first wall provided the opportunity to study the impact of the plasma-facing materials on plasma initiation or breakdown. This study for the first time presents a full experimental characterisation of tokamak breakdown at JET, using all discharges since 2008, covering both operations with a main chamber carbon and a beryllium ITER-like main chamber wall. It was found that the avalanche phase was unaffected by the change in wall material. However, changes in out-gassing by the wall and lower carbon levels resulted in better controlled density and significantly lower radiation during the burn-through phase with the ITER-like wall. Breakdown failures, that usually developed with a carbon wall during the burn-through phase (especially after disruptions) were absent with the ITER-like wall. These observations match with the results obtained from a new model of plasma burn-through that includes plasma-surface interactions. The simulations show that chemical sputtering of carbon is the determining factor for the impurity content, and hence also radiation, during the burn-through phase for operations with a carbon wall. As seen experimentally, with a beryllium main wall, the plasma surface effects predicted by the model do not raise the radiation levels much above those expected for pure deuterium plasmas. With the ITER-like wall, operation with higher pre-fill pressures, and thus higher breakdown densities, was possible, which helped maintaining the density after breakdown.

1. INTRODUCTION

The standard method to initiate plasma in a tokamak is, to ionize pre-filled gas by applying a toroidal electric field via transformer action from poloidal coils. For ITER the available electric field will be limited to low values of $0.33 \mathrm{Vm}^{-1}$, raising considerable interest to understand and optimise the breakdown phase [1]. Pre-ionization by means of microwave heating is seen as an option to provide ITER with a robust and reliable breakdown phase [2,3,4].

It is well-known and reported in the past that impurities have a direct impact on, both unassisted and assisted plasma breakdown phase [2, 5]. At JET un-assisted or Ohmic breakdown has previously been achieved at electric fields as low as $0.23\ \mathrm{Vm}^{-1}$ though with carbon-based plasma facing components [1]. The recent installation of a full metal, ITER-like, first wall [6, 7] provided the opportunity to study directly the impact of the first wall on the breakdown characteristics. This paper will present an experimental characterisation of breakdown at JET, comparing operations with the carbon and ITER-like wall. Here the main emphasis will be on the details in the density dynamics and impurity content.

The Ohmic breakdown process for a tokamak discharge is a complex process that can be divided into a few distinct stages. Firstly, the applied electric field initiates a classical Townsend avalanche phase, in which the main ionization process is due to collisions with electrons accelerated in the electric field [2, 8]. The collisions ensure that the average electron speed will settle at a constant value, while the ionization level, and thus the electron density and current, increases exponentially. Direct losses of electrons along the field lines will affect this phase. The distance along the field lines from the point of ionization to the wall is called the connection length, L, which should be

as long as possible, i.e. an optimum toroidal field with small magnetic poloidal errors. Secondly, as more of the pre-fill gas is ionized, Coulomb collisions will start to dominate over atomic and molecular collisions. The electron-ion collision time is expected to exceed the electron-neutral collision time at ionization levels of roughly 5% [8, 9]. Magnetic flux surfaces can be formed when the plasma current and the associated poloidal magnetic field starts to dominate the poloidal error field, which will further improve the confinement of the particles. All the time the plasma may be expanding and comprising a larger volume. However, the plasma temperature and energy remain low due to ionization and losses from line-radiation by impurities. The plasma needs to burn-through this radiation barrier such that finally sufficient Ohmic flux can be used to further raise the current and heat the plasma, which is the final stage of the breakdown process. The burn-through phase is completed by reducing the impurity line-radiation and yielding complete ionization of the main gas. Note that the avalanche, plasma expansion and burn-through are not necessarily consecutive breakdown phases but processes that could happen simultaneously.

A number of experimental breakdown studies at JET [9] or other devices [10, 2, 4, 5, 11] have been reported in the past with recent studies focusing predominantly on assisted breakdown [12]. Characterising or diagnosing the breakdown phase of a tokamak discharge is not a straightforward task. The process is fast, at JET sometimes a few tens of ms, and not all diagnostics may have sufficient temporal resolution for an accurate analysis. Moreover, many tokamak diagnostics are not tuned to measure the low densities, temperatures or radiation levels in the breakdown phase or only view part of the plasma. Large variations in the breakdown state, often attributed to the influence of the wall, can also complicate comparisons of a small number of discharges. The analysis strategy presented in this paper is to compare a large number of breakdowns under different conditions. All breakdown attempts at JET since 2008, covering the final period with carbon wall operations and the first phase with the ITER-like wall. This will reveal a number of relevant trends and allows a full characterization of JET breakdown providing the basis for the comparison with operations with the new ITER-like wall.

The outline of this paper is as follows. Section 2 will give a short overview on the technical details of plasma initiation at JET, giving characteristic pre-fill pressures, breakdown voltages and time scales. This section will also briefly discuss the issues related to the diagnoses of breakdown. In section 3, the avalanche phase, more particularly its duration, will be characterised. The main parameters that determine the avalanche duration will be studied and the data will be compared with the standard model of a Townsend discharge [2]. Section 4 will show the density, impurity and radiation behaviour, during both the avalanche and the burn-through phase. The impact of de-conditioning events, such as disruptions, on subsequent breakdowns will be discussed and a direct comparison between operations with a carbon and a full-metal, ITER-like, wall will be given. The main conclusions will be discussed in section 5 and compared a new breakdown model that includes impurities and details on plasma-surface interactions [13].

2. ANALYSIS OF PLASMA BREAKDOWN AT JET

A number of features that will be discussed in the next sections can be attributed to the specifics

of the method of plasma initiation at JET. The details of JET breakdown modes will be clarified below. Thereafter the limitations of the diagnosis of the breakdown phase will be discussed pointing out various issues that may result in ambiguity of various key parameters that will be used in the analysis later in the paper.

2.1. INITIATION OF PLASMA AT JET

The vessel is pre-filled with gas using a short puff from a single gas valve at a single toroidal position. Significant differences in pressure between different parts of the torus may exist for several 100ms before the vessel pressure has equilibrated. Usually the pre-fill is timed several 100ms prior to the start of plasma formation, such that the pre-fill pressure is approximately toroidally isobaric. The pre-fill pressures at JET are in the range of 10^{-6} to 10^{-4} mBar. On average the pressure drops slowly after the gas is let into the vessel.

The loop voltage applied to ionise the pre-fill gas in the tokamak vessel is induced via transformer action by poloidal field coils. The main voltage is supplied by the primary coil (P_1) through the centre of the torus, which at JET has 710 turns. The other poloidal field coils can however also provide flux. At JET this is especially true for the vertical field coils (P_v) that are used during the breakdown phase in order to maintain the radial position of the plasma. In this paper the loop voltage, V_{loop}, at breakdown is calculated by adding the effects of these two main coils together, for which the latter contributes usually about 25% in the centre of the torus ($R_o = 3$m). Note that the coils may also determine the main poloidal error field that affects the avalanche phase.

At JET usually two different methods are used to apply the loop voltage. The most common method, called Mode D, pre-magnetises the primary coil slowly with a current (usually in a range of 10 to 30kA). The vessel is pre-filled with gas and the remaining poloidal circuits are tuned such to optimise the error field in the centre of the vessel. By opening the primary circuit the current in the primary coil will decrease with the typical L/R time of the system. The change in flux through the primary coil will generate a loop voltage in the vessel. Depending on pre-magnetization current it induces a loop voltage that can range from about 10V to more than 30V, i.e. electric field in the centre of the plasma of $E(R_o) = 0.53$ and $1.6 \mathrm{Vm}^{-1}$. The second method, is termed Mode B, and directly ramps-up the voltage on the primary coil to values of up to about 15kV. To prevent a too early start of the breakdown a large (vertical) error field is applied by the vertical field coil (P_v), which is stepped down when the required voltage has been reached, starting the avalanche process. The voltages that can be achieved with Mode B are lower than those for Mode D and in the range of 5V to 10V (i.e. $E(R_o) = 0.27$ to $0.53 \mathrm{Vm}^{-1}$)

The first breakdown method, mode D, optimises the error fields after which the voltage is applied to initiate breakdown. The opposite is done by the second method, mode B, that applies the voltage and the breakdown is initiated by reducing the error fields. Hence both methods differ strongly with respect to the poloidal error fields present during the avalanche phase. For Mode D, the poloidal field coils employ a specific combination of the P_1 and P_v coils creating a hexapolar magnetic field null in the centre of the vessel. This ensures a central area with a near toroidal magnetic field and hence a long connection length. The error field for Mode B is not optimised,

except for a few special experiments [1], and thus is expected to be larger than that for Mode D. As discussed below error fields levels at breakdown are rather ambiguous.

At JET the breakdown phase may last from a few 10ms up to several 100ms. The breakdown may not be sustained and create a tokamak plasma. Non-sustained breakdowns can occur because either a failure of the avalanche phase or the plasma is not able to burn-through as will be shown in the following sections. Care is required with the identification of non-sustained breakdowns as in some cases the discharge fails in the early stages due to technical reasons, for example an emergency shut-downs of external power supplies, rather than breakdown physics.

2.2. DATA ANALYSIS AND DIAGNOSIS

In this paper all breakdown attempts over the last period of carbon wall operations from 2008-2009 (Pulse range 70965-78810, in total 6392 entries) are analyses. These are compared with all attempts with the new ITER-like wall in 2011-2012 (Pulse range 80128-83620, in total 2793 entries). Excluded are those that use helium pre-fill or cases for which the time resolution of some key signals were not sufficient to properly monitor the short breakdown phase. Only breakdowns for which the time was allowed for the pre-fill pressure to equilibrate such that it was toroidally isobaric were included. Through-out the paper colour code shown in **table 1** is used in which blue and green represent Mode D breakdown for the carbon and ITER-like wall data, respectively, while black and grey triangles denote Mode B cases. Failed or non-sustained breakdowns are shown by the red and orange symbols.

The statistical approach used in this paper requires that the parameters or signals can be obtained for most of the breakdown attempts and easily analysed (i.e. automatically). For example, the detailed analysis of fast camera images, such as used in ref. [14, 15] would have been too time consuming. Obviously, the diagnostics should also have the required time resolution (i.e. sub 10ms). Diagnosis of the dynamic breakdown phase is not straightforward. Beside the short duration of the breakdown phase, standard assumptions used to analyse diagnostic signals, such as the existence of flux surfaces, or the fact that one observes fully ionized plasma at all, may not hold. Most plasma diagnostics are tuned to record data in parameter ranges that are outside those expected during the plasma formation. A number of issues related to the diagnosis of key breakdown parameters will be discussed below and should be taken into account in the analysis presented in the subsequent sections.

Determining the loop voltage and plasma current may sound straightforward. However, no direct measurement of the loop voltage exists at JET except for the voltage over two restraint rings on the inside of the vacuum vessel (around the primary coils). This only partly captures the flux supplied by the outer poloidal field coils. As explained above, the loop voltage is determined by considering the voltage on each poloidal circuit, the position of the coils and the respective turns. In most cases these are know with a 2ms time resolution. The voltage may also induce currents in passive structures surrounding the plasma, such as the restraint rings around the primary coil, the toroidal base-plate of the divertor and even the vacuum vessel [17]. Only estimates of the currents in the last two of these components exist. Hence the current measurement is an overestimate of

the actual current flowing through the plasma especially when its resistance is still high. Large currents in these passive structures are expected in the early parts of the breakdown phase when the plasma resistance is still high and of similar order of these passive components.

The pre-fill pressure can be measured using penning gauges at various locations in the vessel. Beside the diagnostic uncertainty, the pressure may vary toroidally and even poloidally, making it the most ambiguous breakdown parameter. Uncertainties of ~10-20×10^{-6}mBar should be considered, yielding errors of 100% of more in some cases. Note that after the start of the avalanche process the neutral pressure could be influenced by recycling of ions lost to plasma facing components,
A good measurement of the total radiation is possible. The JET bolometer uses a multitude of view lines that cover the entire vessel and hence always captures the initial plasma, even when small [18]. The diagnostic has a time resolution of 200μs and is used to determine the radiation power during the burn-through phase.

The density can be diagnosed with the JET far-infrared interferometer [19]. The line-integrated density is measured using a vertical channel looking through the centre of the vessel (at R_{LID2} = 2.7m). This measurement may underestimate the density, if the plasma has not yet fully expanded into the view of the diagnostic. Using lateral channels would be ideal; however, these are not always available, limiting the number of entries for our comparison. The interferometer is capable of measuring line-integrated densities as low as $10^{18}m^{-2}$ with a time resolution of 10μs.

The temperature is far more difficult to determine because the breakdown phase is out of the operational range of most standard temperature diagnostics at JET. Indirectly, information on the temperature may be obtained by looking into the line-radiation of the main or impurity ions. The main deuterium Balmer-α (D_α) diagnostic views the plasma with several sight-lines with a temporal resolution of 1ms. Line-radiation, for example CII or CIII or those of other impurities lines such as NIV and OVI, is can be diagnosed using the main impurity spectrometer at JET [20]. The data used in this paper is obtained with a vertical sight-line at R = 2.8m. Similarly as with the line-integrated density, this measurement is affected by the size of the emerging plasma. The time resolution of the main impurity spectrometer is 50ms, and insufficient to study the temporal behaviour of these lines, though it is possible, as we will see later, to obtain a snap-shot during burn-through phase. The signal intensity does not necessarily represent the impurity density but a complex function of the electron and impurity density and the temperature. Other, faster impurity spectroscopy diagnostics exist at JET but these are unfortunately not always available for each breakdown attempt.

Knowledge of the error fields or the connection length is important to understand the avalanche process. It is possible to determine the static poloidal error fields from the settings of the poloidal field coils at breakdown. This field vary considerably over the plasma cross-section making it difficult to assign a single value for the entire plasma. The static picture breaks down if one considers error field dynamics and especially eddy currents. Beside the fact that the fields by the poloidal coils may vary considerably even during the avalanche phase itself, detailed calculations should also include properties of the iron core or the effects of eddy currents induced in passive conducting structures around the plasma. The iron core at JET influences the error field at breakdown [15]

while in other devices even effects due ferromagnetic material surrounding the plasma have been found [16]. A more detailed discussion on electromagnetic analysis of the breakdown conditions at JET can be found elsewhere [14]. In this paper it is shown that it is possible to determine an average value of the connection length for each breakdown attempt, i.e. spatially averaged over the plasma cross-section and averaged over the duration of the avalanche phase.

Mode breakdown models are usually zero-dimensional [2]. In reality relevant parameters vary considerably within the vessel in which the breakdown takes place. As discussed above the pre-fill pressure can vary toroidally but may also differ in the poloidal plane. Both the electric field (i.e. $E = V_{loop}/2\pi R$) and the connection length ($L \mu a\, B(R)/B_{\perp} = a\, B_o \times R / R_o \times B_{\perp}$) vary with the position in the vessel and are expected to be larger on the inside of the vessel, i.e. lower major radius R. Here, B_o is the toroidal magnetic field on axis (R_o) and $B_{\perp}$ is the perpendicular error field, which itself also differs within the poloidal plane. A detailed analysis of for example fast camera images has shown that the plasma, both for Mode B and D, initially forms at the inside of the vessel [14]. It usually encompass the entire vessel by the end of the avalanche phase though in some cases it remains small and may move through the vessel even during the burn-through phase. Fast vertical movements have been found to affect the breakdown process at JET [15]. The 2D dynamics of the breakdown phase will not be considered in detail in this paper. Nevertheless, it will be shown that the two-dimensional nature of breakdown will complicate the characterisation using zero-dimensional breakdown parameters.

3. THE AVALANCHE DURATION

The breakdown process starts with what can be considered a Townsend avalanche discharge, in which the number of electrons, electron density and current increase exponentially, while the electron temperature remains very low (i.e. a few eV). This phase lasts until Coulomb collisions start to dominate and the partly ionized gas starts to behave as plasma. Traditionally the end of the avalanche phase is considered to correspond to the time when the deuterium Balmer-α (D_α) emission peaks. The time it takes to reach this stage has been estimated in ref. [2] to scale as,

$$\tau_{avalanche} \sim \frac{41}{v_{De}(\alpha - L^{-1})} \tag{1}$$

Here v_{De} is the electron drift velocity, directly proportional to E/p_{pre}, α is the first Townsend coefficient again depending on the electric field, E, and the pre-fill pressure, p_{pre}, while L represents the connection length. It is here assumed that the breakdown that takes place in a large vessel can be described by this simple set of zero-dimensional parameters, although these parameters may vary considerably over the duration of the avalanche phase in with the space of the vessel.

Practically it is not easy to determine the D_α emission peak accurately for a very large number of breakdowns at JET. Furthermore the diagnostic line-of-sight may by-pass part of the initial plasma making the determination of time of the D_α emission peak rather ambiguous. At JET the D_α emission peaks roughly at about 30-60kA. In the next section it will be shown that around these values of plasma current the avalanche process has ended as Coulomb collisions start to dominate.

For this study the avalanche phase duration has been determined by the time the plasma current increases from 20 to 45kA ($\tau_{20\text{-}45}$), more accurately corresponding to the characteristic current rise time. The lower level is chosen to avoid issues with signal noise affecting the data. The avalanche time $\tau_{20\text{-}45}$ was determined for all breakdowns in the database. Values for avalanche duration, $\tau_{20\text{-}45}$, vary from 2.5ms from fast Mode D breakdown to over 80ms for slower Mode B cases. A number of expected scalings are tested using these experimental values.

Not unexpectedly, **figure 1a** shows that the avalanche duration scales inversely with the applied loop voltage. Here all 2008-2009 entries are shown that used similar magnetic field ($2.2T < B_o < 2.4T$) and pre-fill pressures ($1.3\ 10^{-5}$ mBar $< p_{pre} < 2.7\ 10^{-5}$ mBar). Because the loop voltage may vary over the duration of the avalanche phase a time-averaged value is used: $V_{20\text{-}45}$.

The avalanche time is also affected by the pre-fill pressure as shown in **figure 1b** again for a selection of Mode D entries with similar loop voltage and magnetic field. Larger pre-fill pressures slow down the avalanche phase. **Figure 1b** can be used to determine the average connection length by fitting equation 1 to the subset of high voltage Mode D breakdowns. For this particular case a value of <L>=900m is obtained. Note that this is an average zero-dimensional value averaged over the entire plasma cross-section and more importantly averaged over the duration of the avalanche phase. Local connection lengths may be considerably longer while the poloidal field coil settings differ between the start and end of the avalanche phase. A similar exercise can be done for different subsets which present a uniform equation of the Mode D average connection length

$$\langle L \rangle_D = \frac{385 \pm 30 \cdot B_o}{1 + 0.0063 \cdot |P_v - 11 P_1|} \qquad (2)$$

Notably, it matters to set the right combination of P_1 (kA) and P_v (A) currents prior to the initiation of breakdown. Static calculations of the poloidal fields show that a central hexapolar null is formed if P_v (A) = 12 P_1 (kA). This is close to the optimum found by equation 2. It is interesting that details of the hexapolar field settings can be found back in the avalanche duration trends found by this database. For these optimum settings the average magnetic error field can be estimated using $<B_\perp> \sim a\ B_o/<L>$ [3]. This gives a value for these optimised settings of ~3mT with a = 1m. Here $<B_{\perp r}>$ is again an average value, not the optimum in the centre of the vessel at the start of the breakdown. In **figure 1c** the determined <L> is shown to scale nicely against the central magnetic field. For several cases in the database non-optimised combinations of P_1 and P_v currents were used for which, as shown by the example in **figure 1c**, a much shorter connection length was found. Although the avalanche was significantly slower, breakdown did not fail even at connection lengths of only $<L>_D \sim 300$m and average error fields of $<B_\perp> \sim 8$mT.

The quality of the fit depends strongly on the range of pre-fill pressures used within the subset of entries, resulting in different error bars in <L> in **figure 1c**. Because the pressure range for low voltage breakdown is limited, a better method would be to fit equation 1 to sub-sets of equal electric field and pressure but different magnetic field. Lower connection lengths are found as expected because the error field for Mode B is usually not optimised at JET. Average error field levels of $<B_\perp> \sim 5\text{-}12$mT are found, about a factor of 2 to 3 larger than for Mode D. The connection

length is again found to depend on the magnetic field (**figure 1c**) as long as subsets with similar electric field are considered. A strong correlation between the estimated connection lengths <L> and the applied loop voltage or electric field is found. In **figure 1d**, the connection length required fitting the experimental avalanche time to equation 1, again for a subset with similar magnetic field and pre-fill pressure is shown. Much shorter connection lengths are found for those Mode B entries that breakdown at with a higher electric field. For Mode B the average connection length is found to scale as,

$$\langle L \rangle_B = 42 \pm 10 \cdot B_o \cdot E_o^{-1} \tag{3}$$

As explained in section 2, Mode B is characterised by the fact that the toroidal electric field is ramped up well before the plasma initiation. During this time, toroidal currents are induced in passive structures that seem to determine the magnetic error field. Currents in the poloidal field coils are usually near zero for Mode B breakdown. The comparison of error field levels for Mode D and B also high-lights another important difference between the two methods. The levels are such for optimised Mode D breakdown that flux surfaces are likely to form early in the avalanche phase (~15kA) but for Mode B higher currents are needed to overcome the error fields (up to 60kA) and an open field line structure is likely maintained through-out the avalanche phase.

With the knowledge on the error field and connection length scaling, one can compare the measured avalanche time, $\tau_{20\text{-}45}$, with that predicted by equation 1. The results are shown in **figure 2** for both carbon and ITER-like wall data. Firstly, in **figure 2b** the scaling is shown assuming only a static error field level for Mode B. Clearly the comparison with equation improves, as shown in **figure 2b**, if the error field is, according to equation 3, assumed to scale with the electric field. A number of other conclusions can be drawn from **figure 2b**. In the first place, most failed breakdowns (open red symbols) fall within the same cloud as those that are sustained. It suggests that, non-sustained, breakdowns at JET are, during the avalanche phase, indistinguishable from those that can be sustained. The next section will analyse what causes breakdown failures at JET. A second observation is that both the carbon and ITER-like wall data follow the same scaling indicating that the avalanche phase was little influenced by the change in wall material. This analysis does not show a significant impact of impurities on the avalanche phase of the tokamak breakdown. The number of entries for Mode B breakdown with the ITER-like wall is spars because few attempts with an isobaric pre-fill pressure were done. More robust Mode B breakdown with the ITER-like wall was obtained with the pre-fill gas injection short before breakdown. In this way the pressure is not equilibrated but it may provide a more direct fuelling of the initial plasma which may have become more important with the ITER-like wall. These breakdown cases are however difficult to compare with for example equation 1, because the value of the pre-fill pressure is ambiguous (i.e. order of magnitude variations exists toroidally).

Finally, the experimental values are generally shorter but this may be due to the slightly different definition of the avalanche durations that are compared. Nevertheless, it is remarkable that the scaling set by equation 1 matches quite well with the experimental observations over a wide

operational range of breakdown voltages, pre-fill pressures and connection lengths. This is even true for breakdown in a parameter range for which according to ref. [2] equation 1 may not be valid and a so-called relativistic approach is required. The scatter seen in **figure 2** is largely due to uncertainties in the input parameters, especially the error bars on the pre-fill pressure, although, deviations may also be caused by effects that are not included in the zero-dimensional avalanche model.

4. DYNAMICS OF DENSITY AND RADIATION

When Coulomb collisions start to dominate, the partly ionized gas starts to behave as plasma. Up to that point it has mainly gained in particle and current density but the temperature remains low. For the temperature to increase it has to raise high enough to fully ionise the main impurities, reducing the energy loss through line-radiation. In this section the transition to the Coulomb and burn-through phase will be discussed and the differences between burn-through with a carbon and ITER-like wall will be shown. This is done by using a specific subset of the breakdown database, consisting of Mode D breakdown with a P_1 pre-magnetisation current in the range of 13 to 16kA, i.e. E_o~0.8V/m or V_{loop}=12V and a corresponding P_v current to obtain an optimum connection length. The same trends are also found for other subsets. The 'dynamics' are visualised by comparing parameters at two different times, approximately at the end of the avalanche phase at $t_1 = 0.031$s and thereafter at a time during the burn-through phase (when most of these entries have their peak in radiation) at t_2=0.051s. These times are specific for the loop voltage used by this subset.

4.1 DENSITY DYNAMICS

In **figure 3** the line-integrated density is plotted as a function of the inverse impedance, the ratio of plasma current, I_p, and loop voltage, V_{loop}. Because most entries have a similar voltage one could also see this as the plasma current variation over the dataset. For the two times distinct patterns are found. For the first time snapshot, a remarkable characteristic of the avalanche process is seen: the obtained density scales with the current. For a higher pre-fill pressure the avalanche process is slower, and hence at t_1 it has developed less current and density, which develop simultaneously. An off-set of ~2kA/V (I_{offset}=24kA) exist for zero plasma suggesting that currents may flow elsewhere beside the plasma, for example in surrounding toroidally conducting structures.

Similarly, although slightly more indirect, one can plot the density data against the calculated resistance, R_p, using,

$$R_p = \frac{V_{loop}}{I_p} - L_p \frac{1}{I_p}\frac{dI_p}{dt} \tag{4}$$

Assuming an inductance of $L_p = 4\mu$H one obtains **figure 4**. Here one should remind that this is the combined resistance of the total system as the currents may not only flow through the plasma but also passive conductors. Nevertheless at the two times different trends are found. At t_1, those cases that have a higher pre-fill pressure a slower and longer avalanche phase results in a lower current and growth rate, hence a higher resistance. Later at t_2 the resistance scales with the density,

thus inversely with the temperature, indicating the Coulomb character of the plasma. A higher density implies a lower temperature, which according to Spitzer's plasma resistivity should give a higher resistivity and thus lower I_p/V_{loop}. Hence, for this subset of breakdowns the transition from an atomic gas to plasma (ge. Coulomb collisions are dominating) has taken place between t_1 and t_2. From figure4a and 4b one may conclude that this transition takes place at approximately ~5kA/V or 60kA. The values in **figure 4** can be compared with the resistance of passive conductors surrounding the plasma such as the divertor support structure (~0.75mΩ) or the JET vacuum vessel (~0.43mΩ) [17].

From **figure 4a** it is also noticeable that all entries fall within a single group, suggesting that the avalanche phase does not develop differently for breakdowns with carbon plasma facing components or an ITER-like wall. The same is true for failed breakdowns. Similar observations were found in the previous section. However, slightly later clearly separate groups are obtained (**Figure 4b**). For the carbon wall entries, those that fail form a separate group above a threshold in resistance and density (i.e. too low temperature). Hardly any ITER-like wall breakdowns failed. For the same density, the resistance is lower for the ITER-like wall. This can be explained by both a lower level of impurities and a higher temperature for a given density during the burn-through phase of an ITER-like wall breakdown.

An interesting question is what determines the density in both the avalanche phase and thereafter? In **figure 5** the density is plotted as function of the pre-fill pressure at the two times. Again a clear Townsend discharge characteristic is found, higher pre-fill pressure slows down the avalanche process and thus one obtains at a fix time t_1 a lower density. Looking at this graph one could argue that for these high pre-fill cases the time t_1 may be too early to characterise the final stages of the avalanche. An optimum is found and for too low pressures the density decreases again, i.e. the avalanche slows down. This is identical to the scaling for the avalanche time, as discussed in section 3. A few breakdown attempts that used too low pre-fill pressures failed during the avalanche process. These failures could be attributed to problems with the gas injection system. But all other failed entries overlay with the main group of sustained breakdowns. But failed entries form a separate group during the burn-through phase (at t_2).

After the avalanche phase (at t_2) the main trend is that the density (and similarly the recycling or D_α intensity) scales with the pre-fill pressure. This is especially true for the ITER-like wall breakdown and highest densities are obtained for the highest pre-fill pressures. For the carbon wall entries, however, the scatter is larger and especially failed breakdowns gained more density than to be expected from the pre-fill. In these cases there is an additional fuelling (of electrons) probably due to out-gassing from the wall and/or the influx of impurities. This effect is more clearly visible if a similar analysis is done for a more robust higher voltage Mode D breakdown subset (i.e. those done to recover from deconditioning events such as disruptions) for which high burn-through densities are obtained with minimum pre-fill pressures. Unfortunately, this subset has a much smaller fraction of ITER-like wall entries and is therefore less suitable for the comparison presented in this paper.

With the ITER-like wall it is possible and also necessary to operate with high pre-fill pressures.

It is questionable whether such high pre-fill pressures would have worked with the carbon wall as increasing the pre-fill and thus the density in **figure 4** would probably have pushed it evidently into the range where it would fail. The different recycling or out-gassing properties between the two wall types also become evident if the density behaviour after the breakdown is observed. For the ITER-like wall there is the tendency to significantly pump the density after breakdown, as can be seen in **figure 6**, while opposite is the case for the carbon wall. Without additional fuelling, out-gassing maintains the density with the carbon wall. Similar density pump-out behaviour as with the ITER-like wall were seen with the carbon wall shortly after strong Beryllium evaporations. It can be prevented by both a high pre-fill pressure, and thus creating a high density right after the burn-through phase, and by starting as early as possible with additional fuelling shown by the other ITER-like wall example in **figure 6**.

4.2 IMPURITIES AND RADIATION

Here the CIII line-intensity CII ($\lambda_{CIII} = 977$Å) at t_2 is used to characterise the level of carbon in the burn-through phase which is compared with the radiation power (P_{rad}) and line-integrated density at the same time. One should note, however, that for most entries of this data subset, the CII ($\lambda_{CII} = 904$Å) and CIII ($\lambda_{CIII} = 977$Å) line emission and radiation peak slighly before $t_2 = 0.051$s, showing that the main burn-through has already been achieved.

In **figure 7** it is shown that typically, for carbon wall breakdown higher densities and radiation are obtained due to the higher levels of carbon. For the ITER-like wall the carbon levels during breakdown are significantly lower (about an order of magnitude) and the high densities are purely due to the pre-fill pressure that was used. For the ITER-like wall the radiation intensity (P_{rad}/n_e^2) is typically a factor 5 lower for carbon wall. The absence of any burn-through failures already indicates that this clearly improves breakdown with the ITER-like wall.

Also for the ITER-like wall the dominant factor determining the radiation level during the burn-through phase was the carbon. The highest radiation intensities were mostly obtained for cases with a high carbon level. The highest level of carbon were found at the start of the operation with the new ITER-like wall, after which it decreased significantly, creeping up slightly during the high power operations at the end of the experimental campaign [21].

Within the carbon data set there is a large variation in the oxygen level, which was high at the start of operations 2008 and dropped significantly thereafter. However, no significant trend of breakdown with respect to the oxygen level was found and the level of carbon seems to dominate the burn-through physics. This contrasts with the impact of nitrogen which has been used in several experiments with the ITER-like wall in order to increase the divertor radiation, decreasing the target temperatures [22]. In **figure 8** the radiation and nitrogen level during the breakdown of a series of ITER-like wall discharges is shown. Most of the highest radiation points with the ITER-like wall seen in **figure 7** are obtained during or after N seeding experiments. The use of nitrogen increases the radiation to levels to approaching those at which burn-through failures would be expected. There is a legacy of about two dozen discharges or one day of JET operations after the use of nitrogen has ceased.

4.3 THE TEMPERATURE IN THE BURN-THROUGH PHASE

When the plasma temperature increases, the line-emission by impurities does too, until a peak is reached, after which for higher temperatures the line-emission will decrease. For CIII ($\lambda_{CII} = 977$Å) the emission peaks at 5eV, thus at this specific time of peak emission, the temperature should be well determined. Indirectly one could also obtain information on the temperature calculating the plasma resistivity using equation 4 and assuming that according to Spitzer it scales as: $R_p \mu Z_{eff} T_e^{3/2}$. Here T_e is the electron temperature and Z_{eff} is the effective charge of the plasma, a measure of the average impurity fraction. In **figure 8** the resistivity is calculated using equation 2 at the time of the CIII emission peak for all carbon wall entries. Note, this is not exactly at $t_2 = 0.051$s as used in the other graphs, but often earlier or sometimes slightly later. Because at this time the temperature should be the same $T_e = 5$eV for all points, one would expect the resistivity to scale with CIII intensity normalised to the density. The latter is an approximation for Z_{eff} assuming that carbon is the dominant impurity. Although a faint trend may be visible for those discharges with higher levels of carbon, for cleaner plasmas such a scaling is not present. A wide range of resistances is possible for similar carbon levels. Moreover, the resistivity for a $T_e = 5$eV and $Z_{eff} = 1$ plasma is already significantly higher (0.59mΩ) than the calculated values in **figure 8** and much higher temperatures (10-50eV) are needed to explain the resistivity values obtained using equation 2.
These discrepancies indicate that it is not possible to characterise the plasma with a single temperature at this stage. The method using the resistivity provides a volume average value, with higher peak values in the plasma centre and a colder edge from which the line-emission originates. Already this early in the plasma formation a temperature and likely also current and electron density profiles would have formed.

5. DISCUSSION AND CONCLUSIONS

A considerable effort has been initiated to improve the understanding of plasma breakdown in large tokamaks. The analysis presented in this paper attempts to provide a general experimental characterisation of both the avalanche as well as the burn-through phase of plasma breakdown at JET. It has also high-lighted a number of issues that require further attention.

It was found that the avalanche phase at JET could be reasonably well described by a zero-dimensional Townsend model. The dependency on the density and current obtained as a function of the pre-fill clearly show the Townsend character of this phase. However, the comparison fails for some low voltage breakdowns. The detailed dynamics of the initial plasma within the large vessel, its expansion but also its radial and vertical movement may have to be considered. It is also thought that the error field dynamics and the influence of eddy currents induced in the surrounding passive structures, become important and efforts are undertaken to model this more accurately [14, 15].

In general failures in the avalanche phase are rare. For operation with the carbon wall only a small fraction (a few percent) failed in the avalanche phase, mainly due to too low or zero pre-fill pressure, while >85% of all non-sustained breakdown failures occurred in the burn-through phase. Mostly such events could be connected to deconditioning problems, for example disruptions [24].

All other failures were found to be due to technical problems, like an emergency shut-down of coil power supplies. For the period of carbon wall operations considered in the analysis (2008-2009), 8.8% of all discharges had a failed breakdown, while this dropped to 2.7% with the ITER-like wall. Almost all of these were due to technical issues while failures due to burn-through problems were nearly absent with the ITER-like wall (i.e. one case observed being a low voltage Mode B during a session with N seeding).

The ITER-like wall was found to have a profound impact on plasma breakdown. The avalanche phase was unaffected and seems to be dominated by the pre-fill pressure and its composition (i.e. type of gas). But as expected, the burn-through phase strongly depends on the plasma facing material. The recycling or out-gassing properties and the levels of main impurities such as carbon changed significantly with the introduction of the ITER-like wall, affecting the density and radiation in the burn-through phase. The highest radiation levels during the burn-through phase of ITER-like wall breakdowns were obtained at the start of operation, when the carbon levels were higher, but also during and after the use of N as extrinsic impurity. No clear trend was found with respect to the oxygen content of the plasma. The lower radiation efficiency of beryllium in comparison to carbon in combination with the fact the peak radiation is at lower temperature, allows for a faster burn-through. For the carbon wall, out-gassing and impurity release were responsible for a large part of the electron density build up during the burn-through phase. In contrast, this component was almost absent with the ITER-like wall. During the burn-through phase the density was determined by the amount of pre-fill gas making it more reproducible. A higher dynamic retention with the ITER-like wall made it however more difficult to sustain the neutral and plasma density. The changes in breakdown with the ITER-like wall did not lead to a substantial reduction in flux-consumption.
A new model of plasma burn-through including plasma-surface interaction effects has been developed [13]. Impurity levels during the breakdown in this model are self-consistently determined by the plasma-surface interactions. These are determined via the impurity sputtering yields and it assumes an exponential decay model of the deuterium recycling coefficient. The rate and power coefficients in the Atomic Data and Analysis Structure (ADAS) package are adopted to solve energy and particle balance. Neutral screening effects are taken into account according to particle species, and the energy and particle balances are calculated. The burn-through simulations show good quantitative agreement with carbon wall JET data [13]. In the previous sections it was shown that the avalanche phase seems to be independent of the wall conditions. The simulations show that with a carbon wall chemical sputtering allows the carbon content to build up during the formation of the plasma, dominating the radiation. While the model shows that physical sputtering of beryllium does not raise radiation levels much above those obtained with pure deuterium plasmas [23], similar as seen in the experimentally.

Failure of the burn-through phase occurs when the radiation power is higher than the power obtained from Ohmic heating. Modelling showed that, for a given electric field (eg. Ohmic heating) this will occur at a specific level of pre-fill pressure. Because the radiation scales with the particle density which, as shown in **figure 3b**, depends on the pre-fill. Obviously, this limit is reduced for cases with higher impurity content. Note that indeed for the ITER-like wall the experiments

showed that it is easier to operate at much higher pre-fill pressures than with the carbon wall (see **figure 3b**). The dependency of the burn-through limit on electric field and pre-fill pressure can be added to the criteria for a successful avalanche. Interestingly, the model shows that even for pure deuterium plasmas, the maximum pre-fill is lower than the limit at which the avalanche would fail. Hence, at too high a pre-fill the breakdown would fail, not because the avalanche fails but first because it will not be able to burn-through. Note, that for the ITER-like wall much higher pre-fill pressures could be used than with the carbon wall.

With the ITER-like wall successful plasma burn-through could be achieved with higher pre-fill pressures and higher densities. Even more so, the much lower out-gassing with the ITER-like wall required breakdown at higher pre-fill pressures and additional fuelling to maintain the density right after breakdown. This in turn may have complicated low voltage breakdown (Mode B) at JET for which the Townsend avalanche criteria allow only a limited pre-fill pressures range.

The analysis showed that it is possible to give a rough characterization of the avalanche phase with a single set of zero dimensional parameters. However, in other cases indications are found that profiles may have to be taken into account. A signing a single connection length to a breakdown is also not straightforward and it might be better to consider the multi-dimensional error field map in stead. Moreover, the dynamics of the error field and the influence of eddy currents need to be taken into account. The plasma may furthermore expand and move through the vessel, influenced by surrounding field coils and its interaction with the plasma facing components. These issues need to be understood properly in order to more accurately describe and model breakdown in large tokamaks.

ACKNOWLEDGEMENTS

This research was funded partly by the European Communities under the contract of Association between EURATOM and FOM and was carried out within the framework of the European Fusion Development Agreement. The views and opinions expressed herein do not necessarily reflect those of the European Commission.

REFERENCES

[1]. A.C.C. Sips, et al., Nuclear Fusion **49** (2009) 085015.
[2]. B. LLoyd, et al., Nuclear Fusion **31** (1991) 2031.
[3]. B. Lloyd, et al., Plasma Physics and Controllled Fusion **38** (1996) 1637.
[4]. R. Yoshino, et al., Plasma Physics and Controllled Fusion **39** (1997) 205.
[5]. E.A. Lazarus, et al., Nuclear Fusion **38** (1998) 1083.
[6]. G.F. Matthews et al., Physica Scripta **T145** (2011) 014001.
[7]. V. Philipps, et al., Fusion Engineering and Design **85** (2010) 1581.
[8]. R. Popoular, Nuclear Fusion **16** (1976) 37.
[9]. A. Tanga, et al., in Tokamak Start-up (Ed. H. Knoepfel) Plenum Press, New York and London (1986) p159.
[10]. M. Valovic, et al., Nuclear Fusion **27** (1987) 599.

[11]. G.L. Jackson, et al., Physics of Plasmas **51** (2010) 056116.
[12]. G.L. Jackson, et al., Nuclear Fusion **51** (2011) 083015.
[13]. H.T. Kim, A.C.C. Sips and W. Fundamenski, Nuclear Fusion **52** (2012) 103016
[14]. F. Maviglia, et al., Fusion Engineering and Design (2011) 675.
[15]. R. Albanese, et al., Nuclear Fusion **52** (2012) 123010.
[16]. J. Kim, et al., Nuclear Fusion **51** (2011) 083034.
[17]. R. Albanese, et al., Nuclear Fusion **44** (2004) 999.
[18]. A. Huber, et al., Fusion Engineering and Design **82** (2007) 1327.
[19]. A. Boboc, et al., Review of Scientific Instruments **77** (2006) 10F324.
[20]. A. Czarnecka, et al., Plasma Physics and Controllled Fusion **53** (2011) 035009.
[21]. S. Brezinsek, et al., *Fuel Retention Studies with the ITER-likeWall in JET*, Contribution to the 24rd IAEA Fusion Energy Conference (San Diego 2012) EX/4-1
[22]. C. Giroud, et al., *Nitrogen seeding for heat load control in JET ELMy H-mode plasmas and its compatibility with ILW materials*, Contribution to the 24rd IAEA Fusion Energy Conference (San Diego 2012) EX/P5-30
[23]. H.T. Kim, A.C.C. Sips and W. Fundamenski, *Plasma-surface interaction effects on plasma burn-through in JET*, accepted for publ. in Journak of Nuclear Materials (2013)
[24]. P.C. de Vries, et al., Plasma Physics and Controllled Fusion **54** (2012) accepted

Breakdown type	**Label**
With carbon wall	
Sustained Mode D	●
Non-sustained Mode D	○
Sustained Mode B	▲
Non-sustained Mode B	△
With ITER-like wall	
Sustained Mode D	●
Non-sustained Mode D	○
Sustained Mode B	▲
Non-sustained Mode B	△

Table 1: Colour coding and labels used to indicated the various types of breakdown though-out the paper.

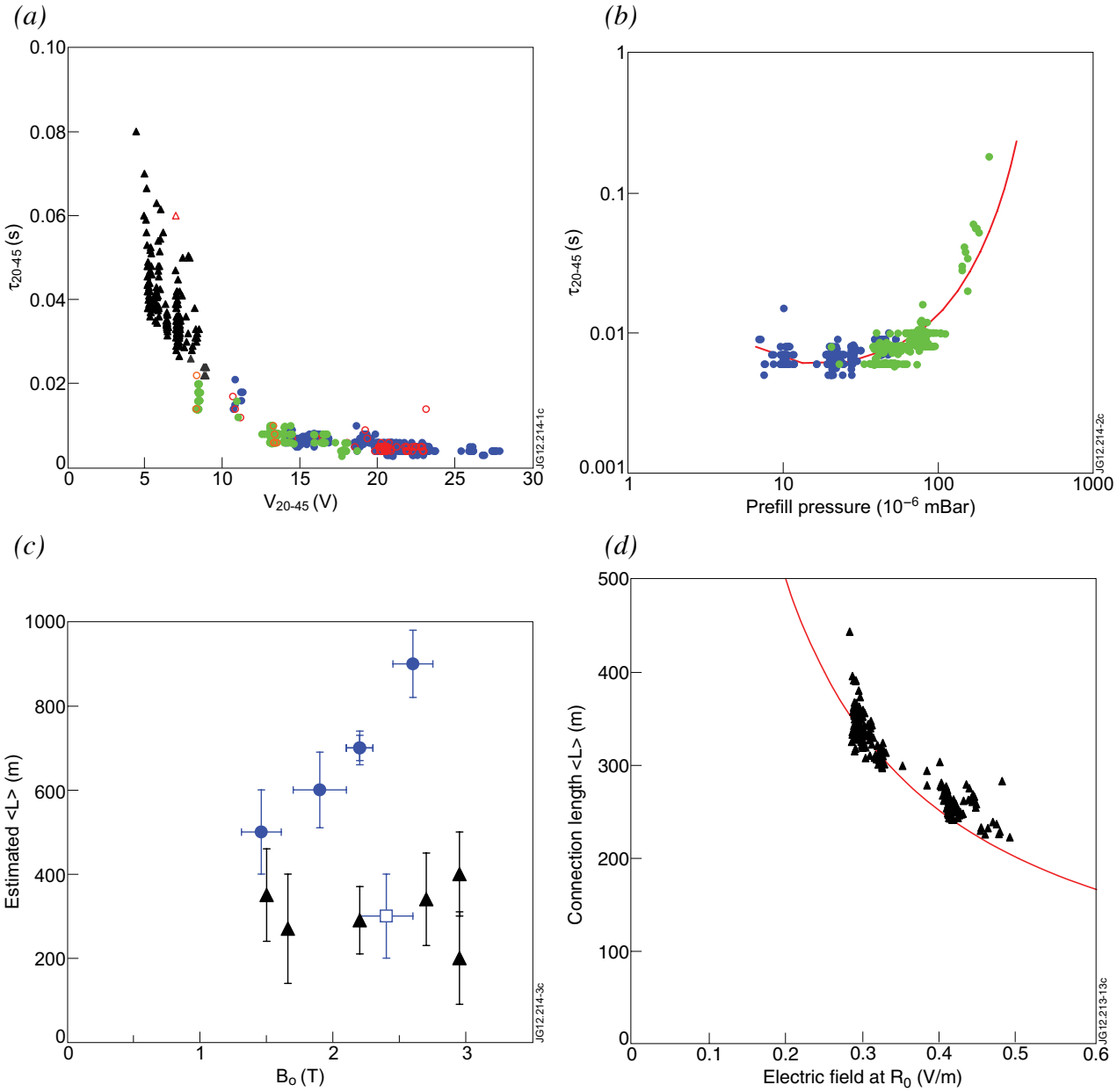

Figure 1: a) Scaling of the measured avalanche time $\tau_{20\text{-}45}$ as a function of the averaged loop voltage $V_{20\text{-}45}$ over the duration of the avalanche time for a select set of discharges with ($2.2T < B_0 < 2.4T$) and pre-fill pressures (1.3×10^{-5} mBar $< p_{pre} < 2.7\times10^{-5}$ mBar). b) Scaling of the avalanche time $\tau_{20\text{-}45}$ as a function as a function of the pre-fill pressure, for a subset of Mode D breakdowns using $2.1T < B_0 < 2.3T$ and a P1 pre-magnetization current of 14kA to 16kA (E_0~0.82V/m). The curve shows the calculated avalanche time using $E = 0.82$V/m and <L> = 900m. c) The dependency of the determined average connection length <L> as a function of the magnetic field. Values for Mode D breakdown with an optimum field-null are shown using the closed blue circles. For one magnetic field value, <L> was determined for a non-optimised field-null (open blue square). The black triangles show values for Mode B cases with different magnetic field but also different electric fields. All have E_0~0.3 Vm^{-1} except for those with higher values as indicated in the graph. The error bars indicate the range of the magnetic fields to select the subset on which the fit is carried out and the quality of the fit. The blue dashed and black long dashed lines give the scale from equations 2 and equation 3 (with E_0=0.3 Vm^{-1}), respectively. d) Scaling of the average connection length <L> with the electric field, for a subset of Mode B discharges with similar magnetic field ($2.5T < B_0 < 2.8T$) and pre-fill pressures (1.3×10^{-5} mBar $< p_{pre} < 2.7\times10^{-5}$ mBar). The scaling from equation 3 (using $B_0 = 2.65T$) is indicated by the dashed line.

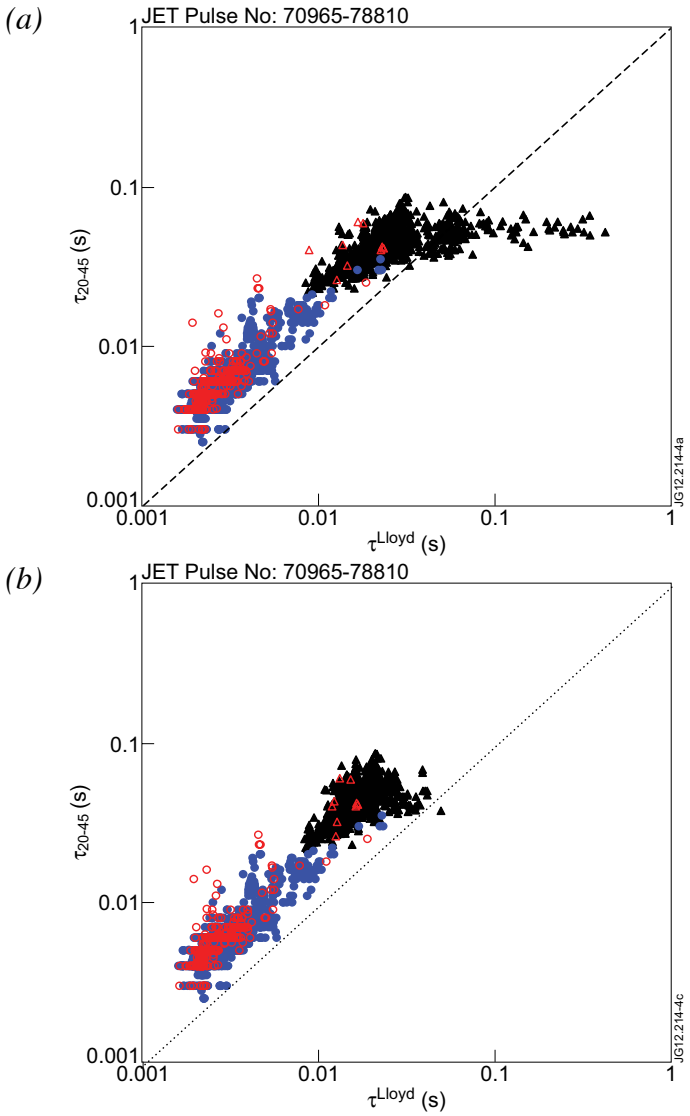

Figure 2: A comparison of the measured avalanche duration and that determined with equation 1 for both carbon wall data and ITER-like wall data. a) assumes a fixed error field level for Mode B data while in b) it scales according to equation 3, inversely with the electric field.

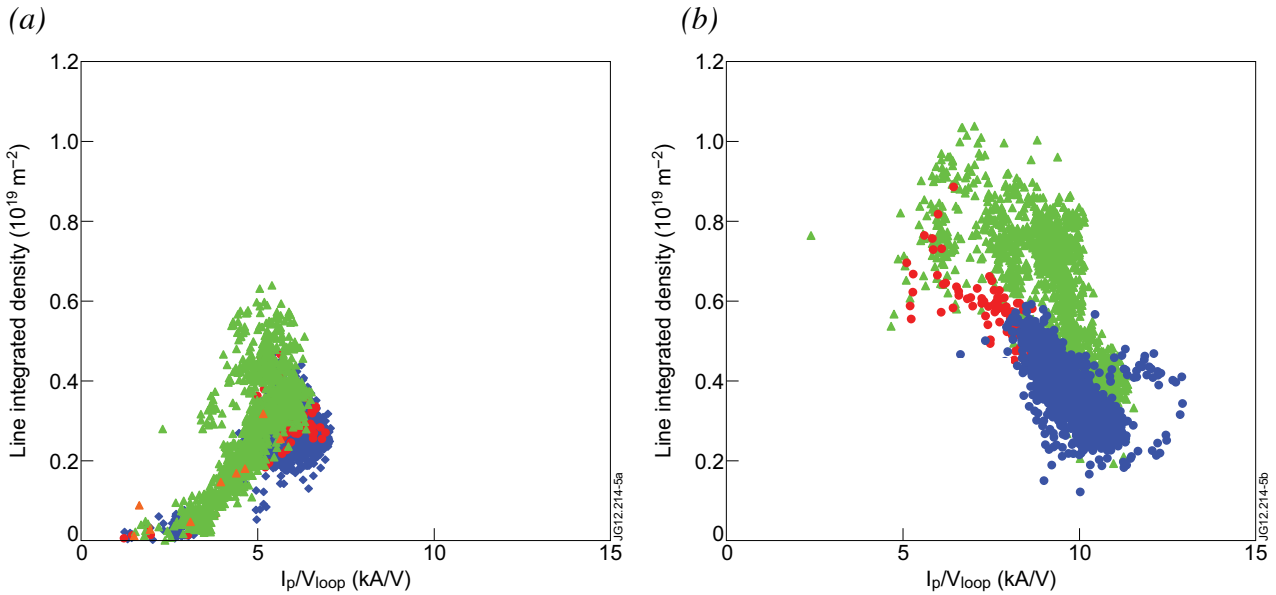

Figure 3: The line-integrated density as a function of the inverse impedance I_p/V_{loop} at a) at t_1=0.031s and b) at t_2=0.051s.

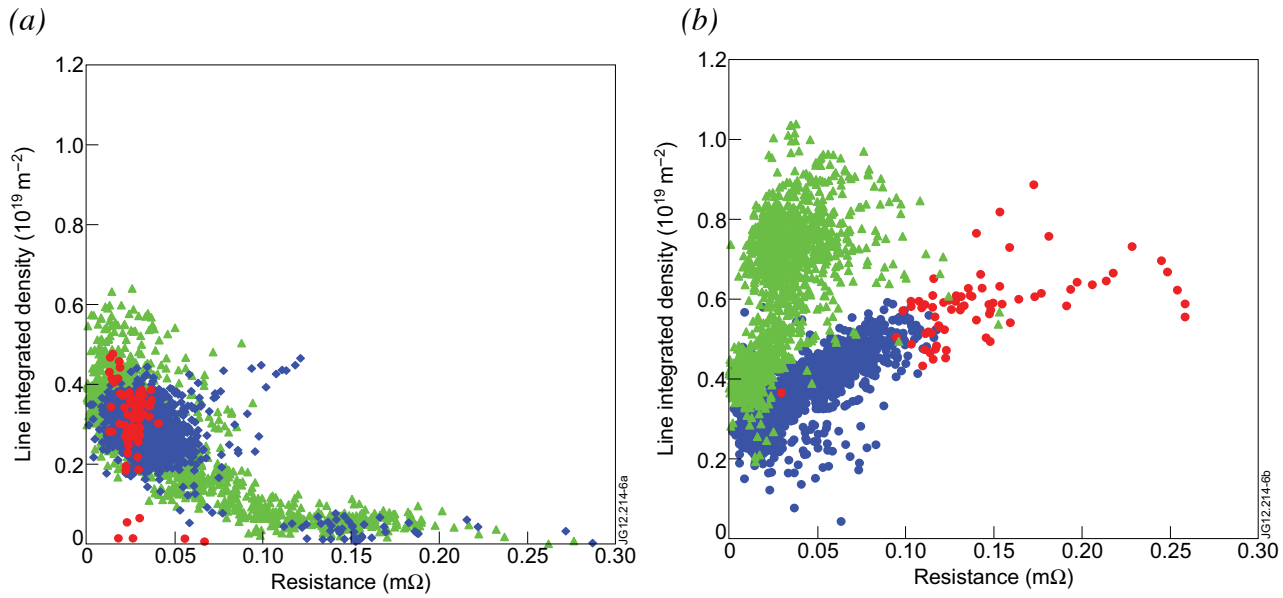

Figure 4: The line-integrated density as a function of the calculated plasma resistance using equation 2 at a) at t_1 = 0.031s and b) at t_2 = 0.051s.

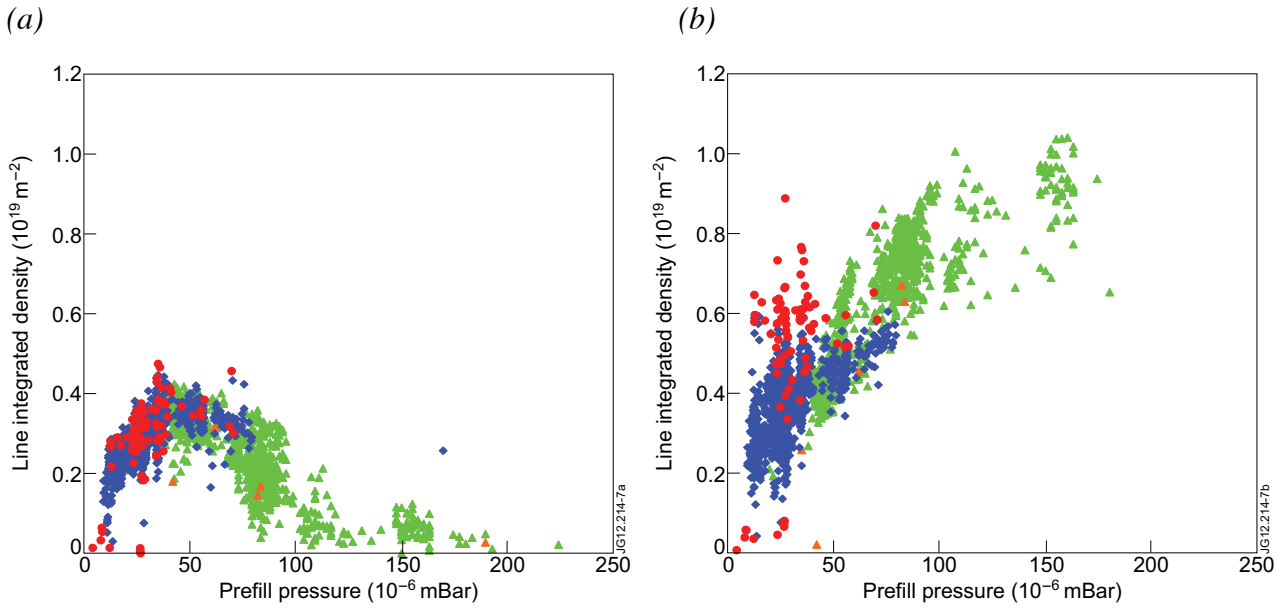

Figure 5: The line-integrated density as a function of the pre-fill pressure at a) at t1=0.031s and b) at t2=0.051s.

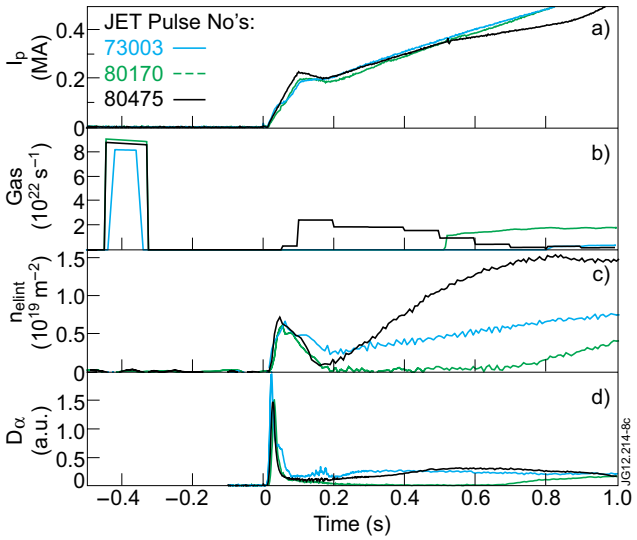

Figure 6: A comparison of the density behaviour after a carbon wall breakdown and two ITER-like wall examples with similar breakdown voltages. a) The plasma current. b) Deuterium gas dosing (in electrons per second), including the pre-fill phase, 400ms prior to the start of breakdown. c) The line-integrated density. d) The Dα intensity giving an indication of recycling.

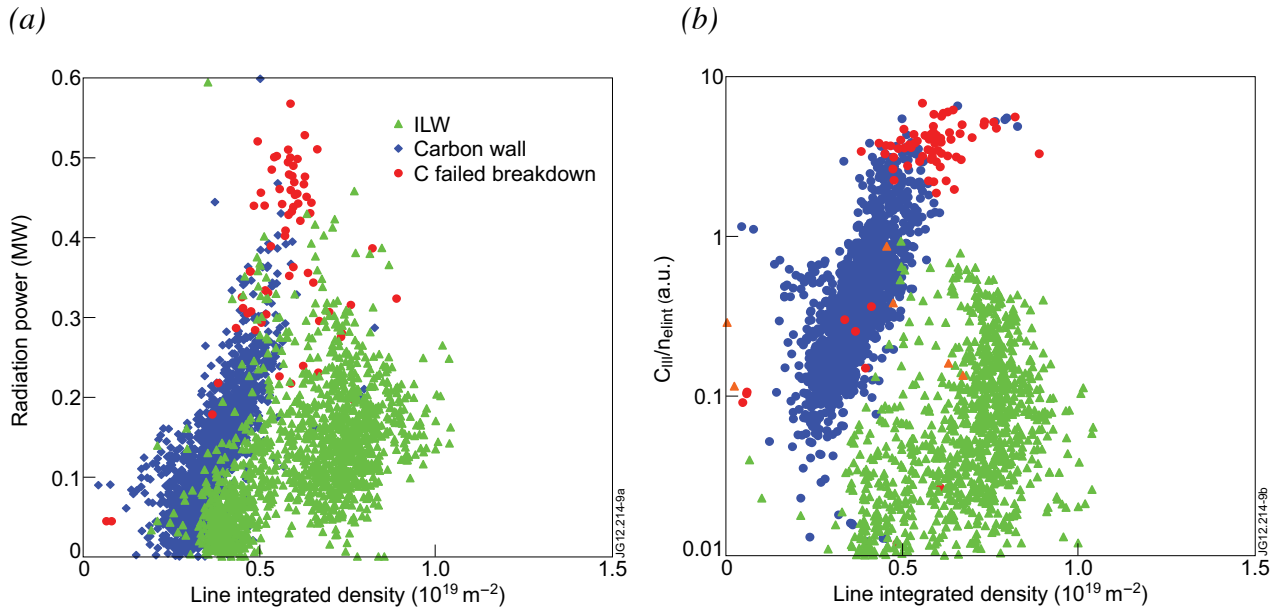

Figure 7: a) The radiation and b) carbon level (i.e. the CIII (λ_{CIII} = 977Å) line-intensity, normalised to the density) versus the line-integrated density. Both take at the same time t_2 = 51ms.

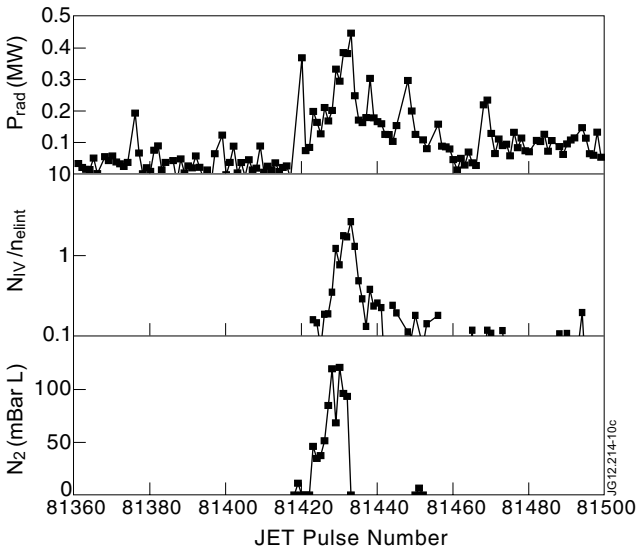

Figure 8: a) The radiation during the burn-through phase (at t_2 = 0.051s) for a series of JET breakdowns with the ITER-like wall. b) The nitrogen level (i.e. the NIV (λ_{NIV} = 765Å) line-intensity normalised to the density). c) The total amount of N_2 fuelling per discharge in mBar liters. The breakdown radiation rises when the N_2 seeding experiments start. Some high-radiation peaks (indicated by the red circle) are identified as contaminated first pulses of the day.

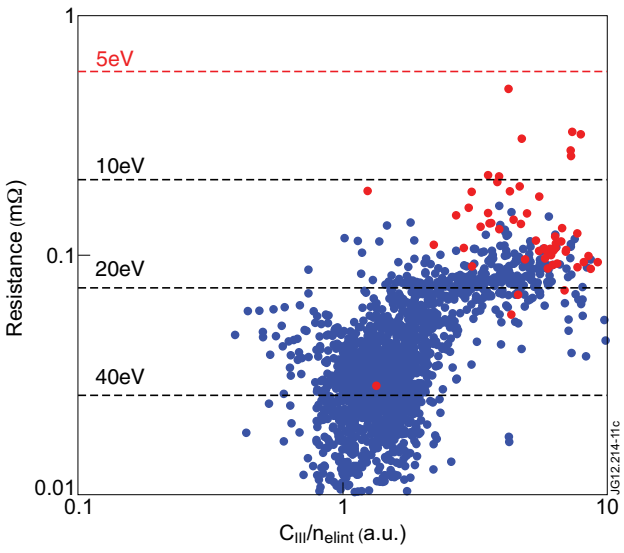

Figure 9: a) The calculated resistivity using equation 4 at the time of peak CIII line-emission (λ_{CIII} = 977Å) for carbon wall Mode D breakdowns only. Assuming Spitzer resistivity and Z_{eff} = 1, corresponding electron temperatures are indicated by the dashed lines.